Sciencexpress Research Articles

Structure of the large ribosomal subunit from human mitochondria

Alan Brown,* Alexey Amunts,* Xiao-chen Bai, Yoichiro Sugimoto, Patricia C. Edwards, Garib Murshudov, Sjors H. W. Scheres, V. Ramakrishnan†

MRC Laboratory of Molecular Biology, Francis Crick Avenue, Cambridge CB2 0QH, UK.

*These authors contributed equally to this work.

†Corresponding author. E-mail: ramak@mrc-lmb.cam.ac.uk

Human mitochondrial ribosomes are highly divergent from all other known ribosomes and are specialized to exclusively translate membrane proteins. They are linked with hereditary mitochondrial diseases and are often the unintended targets of various clinically useful antibiotics. Using single-particle electron cryomicroscopy, we have determined the structure of its large subunit to 3.4 angstrom resolution, revealing 48 proteins, 21 of which are specific to mitochondria. The structure unveils an adaptation of the exit tunnel for hydrophobic nascent peptides, extensive remodeling of the central protuberance, including recruitment of mitochondrial tRNA^{Val} to play an integral structural role, and changes in the tRNA binding sites related to the unusual characteristics of mitochondrial tRNAs.

The human mitochondrial (mt) genome encodes 13 essential proteins of the oxidative phosphorylation (OXPHOS) complexes of the inner mitochondrial membrane. These proteins are translated by a dedicated set of ribosomes (mitoribosomes). The mitoribosome has a sedimentation coefficient of 55*S* and consists of a large (LSU, 39*S*) and small (SSU, 28*S*) subunit. These subunits contain a 16*S* rRNA and 12*S* rRNA respectively, and no 5*S* rRNA (*1*). They differ from cytoplasmic and bacterial ribosomes in having a high protein to RNA ratio. All proteins synthesized by human mitoribosomes are hydrophobic, integral membrane proteins and some require prosthetic groups for folding and functioning. Unlike their cytoplasmic counterparts, human mitoribosomes are permanently tethered to the mitochondrial inner membrane through the LSU (*2*). Mitochondrial diseases affect >1 in 7500 live births (*3*) with defects of mitochondrial translation responsible for a subgroup associated with decreased OXPHOS activity [reviewed in (*4*)]. Cancer cells have amplified OXPHOS capacity and elevated mitochondrial protein translation compared with adjacent stromal tissue (*5*). Specific inhibition of mitoribosomes has successfully induced selective cytotoxicity in leukemia cells (*6*) establishing mitoribosomes as drug targets for cancer. Furthermore, mitoribosomes are often the unintended targets of various clinically useful antibiotics that target protein synthesis by bacterial ribosomes (*7*).

The high-resolution structure of the yeast mt-LSU revealed a major remodeling of mitoribosomes compared to bacterial and cytoplasmic ribosomes (*8*). However, yeast mitoribosomes are themselves very distinct from mammalian mitoribosomes. Structural information for mammalian mitoribosomes is limited to a ~5 Å reconstruction of porcine LSU (*9*) and a ~7 Å structure of bovine 55*S* (*10*) that suggested substantial differences with the yeast mitoribosome. Here we report a stereochemically refined, nearly complete model of human mt-LSU at 3.4 Å resolution, achieved by a combination of rapid biochemical purification in mild conditions (*11*), and recent developments in data processing (*12*) and model building (*8*). We identify 16 more proteins than in the previous porcine model (*9*) and reveal mt-tRNA^{Val} as a key structural component of the mitoribosome.

Overall structure of human mt-LSU

Intact human mitoribosomes were purified from human embryonic kidney (HEK293) cells within 28 hours of mitochondria disruption (*11*) and visualized using single-particle electron cryomicroscopy (cryo-EM) (fig. S1). The data were processed resulting in a reconstruction that extends to 3.8 Å (fig. S1). The SSU displays considerable conformational heterogeneity with respect to the LSU, so the SSU map could not be interpreted with an atomic model. The use of a soft mask over just the LSU improved its map quality and overall resolution to 3.4 Å (fig. S1D).

The model of the human mt-LSU contains two structural RNA molecules (16*S* mt-LSU rRNA and the newly identified mt-tRNA^{val}), as well as a tRNA bound to the E site (fig. S3), and 48 proteins, of which 21 are specific to mitochondria (table S2, Fig. 1, and fig. S4). Five additional short protein elements remain unassigned, but probably correspond to unbuilt protein extensions. The mt-LSU is highly protein-rich with over two-thirds of the total mass of 1.7 MDa consisting of proteins, of which 0.54 MDa can be attributed to mitochondria-specific elements. This gives the human mt-LSU a distinct morphology from both bacterial ribosomes and yeast mitoribosomes (figs. S5 and S6). The connectivity between proteins has also expanded, with each protein making an average of 4.9 contacts (fig. S7). Both the average mass of the mitoribosomal proteins and the number of inter-protein contacts exceeds those of the mammalian cytoplasmic ribosome (*13*).

While the protein composition has substantially increased, the length of mt-LSU rRNA (1559 nucleotides) has halved compared to bacterial 23*S* rRNA. Contraction has occurred in all domains (figs. S8 to S10). Using base-pair information extracted from the structure we have constructed a revised secondary structure diagram of mt-LSU rRNA (fig. S7). In contrast to yeast mitoribosomes where rRNA deletions are minor and primarily occur at the tunnel exit (*8*), deletions of human mitoribosomal RNA are numerous and evenly distributed. The reduction is frequently a result of shortening surface exposed helices. The extant regions are bridged by 37 short 'bypass segments' often of just 2-4 nucleotides (fig. S9). When internal helices are excised, the location of downstream rRNA elements typically remains unaffected. For example, helices 95-97 (including the sarcin-ricin loop that is essential for GTP-catalyzed steps of translation) have conserved locations despite the absence of connecting stem h94, due to partial stabilization by mitochondria-specific proteins (fig. S11). Truncation of rRNA and the absence of 5*S* rRNA have presumably contributed to the loss of uL5, bL25, and bL31 from the mt-LSU compared to bacterial ribosomes (fig. S8). However, uL6 is absent despite strong conservation of the rRNA to which it binds.

Mitochondria-specific protein elements

Proteins homologous to those in bacteria are, on average, ~60% larger in the human mt-LSU. The extensions are shorter and not conserved with those in the yeast mitoribosome (*8*) (fig. S4). Although some of the extensions fill voids left by rRNA deletions, the amount of rRNA replacement by protein extensions is small (fig. S12). Some extensions protrude

into solvent, but predominantly they interact with mitochondria-specific protein elements (table S3).

Mitochondria-specific proteins are peripherally distributed over the solvent accessible surface of the ribosome (Fig. 1) with clusters at the central protuberance, the L7/L12 stalk and adjacent to the polypeptide exit site. They have generally adopted new positions rather than compensating for lost rRNA (Fig. 1 and fig. S12), although a large deletion in domain III (h53-h59) is occupied by a ~100 kDa heterodimer of mL37 and mS30 (fig. S12). Other mitochondria-specific proteins that compensate for lost rRNA (mL41, mL42, mL49, and mL51) are relatively small proteins that help stabilize bypass segments. The effect of not compensating all lost rRNA is an architecture less compact than cytoplasmic ribosomes. Despite the increased porosity, the rRNA accessible to solvent has reduced by 52% compared to bacterial ribosomes. This decrease can only partially be accounted for by reduced rRNA content (41%), with new protein elements contributing by burying 32,500 Å^2 of rRNA surface. This agrees with the hypothesis that accretion of mitochondria-specific elements shield the rRNA from reactive oxygen species (*14*) that are elevated in mitochondria as a by-product of OXPHOS and are a major source of RNA damage.

Two of the proteins (mS30 and bS18a) were previously classified as components of the mt-SSU (*10*, *15*). The presence of three sequence variants of bS18 had led to suggestions that differential incorporation of bS18 variants generates a heterogeneous population of mitoribosomes (*16*). However, the identification of bS18a in the mt-LSU suggests that bS18 variants may not promote structural diversity, but represent a duplicated fold incorporated into distinct locations of the mitoribosome.

Mt-tRNA^{Val} is a part of the central protuberance

The map of human mt-LSU reveals a density corresponding to an L-shaped RNA molecule located at the top of the central protuberance in a position similar to that occupied by 5*S* rRNA in cytoplasmic ribosomes (fig. S13). The RNA component was also reported in the porcine mitoribosome (*9*). We biochemically extracted the RNA molecule from purified human mt-LSU (fig. S13A) and using deep RNA-sequencing (*11*) identified it as mt-tRNA^{Val} (Fig. 2). A structural model of this tRNA agrees well with the density (fig. S13, B to D).

That mt-tRNA^{Val} becomes incorporated over other tRNAs may result from its location in the mtDNA chromosome (*17*). The mt-tRNA^{Val} gene is flanked by the two mt-rRNA genes, which are transcribed together as a polycistronic transcript (*18*) (fig. S13E). In bacteria, it is the 5*S* rRNA gene that is located adjacent to the rRNA genes and cotranscribed with them as part of a polycistronic message (*19*). As with 5*S* rRNA in bacteria, mt-tRNA^{Val} would be present in stoichiometric amounts after processing, and spatially coincident for incorporation into the LSU. The 12*S* rRNA-tRNA^{Val}-16*S* rRNA organization is almost invariant amongst vertebrates (*20*).

Remodeling of the central protuberance

The central protuberance of the human mt-LSU is substantially different from other ribosomes, including the yeast mitoribosome, as a result of the absence of 5*S* rRNA and its associated proteins (uL5, bL25 and bL31) coupled with the incorporation of mt-tRNA^{Val} and mitochondria-specific proteins (Fig. 3). Despite the remodeling, two functions of the central protuberance are maintained, through entirely mitochondria-specific elements; an interaction with the head of the small subunit, and with tRNAs bound to the ribosome (fig. S14). This suggests that the interdependence between inter-subunit communication and the fidelity of translation (*21*) is preserved in mitoribosomes. Due to functional flexibility at the interface, we could not assign the density mediating these functions to specific elements. It is coordinated by an entirely mitochondria-specific cluster (mL40, mL46, mL48) that is bound to the base of the central protuberance (uL18, bL27, mL38, mL52, and ICT1) through mt-tRNA^{Val} (Fig. 3B) and by an unknown mitochondria-specific protein of the small subunit (fig. S14). This region is likely to undergo structural rearrangement during translation [reviewed in (*22*)], for which mt-tRNA^{Val} might provide the necessary plasticity. In the yeast mitoribosome this function could be realized through unique rRNA expansion segments (*8*).

Mt-tRNA^{Val} is located at the top of central protuberance with the acceptor stem exposed to solvent and less well resolved than the anticodon arm, which is ordered due to contact with uL18, mL38, mL40, and mL48 (Fig. 3, C and D). mL40 binds through a 70 Å long helix that stretches from the tip of the acceptor arm to the anticodon stem where it makes base-specific interactions in the major groove. uL18, mL38 and mL40 primarily interact with the phosphate backbone. The core architecture of the central protuberance is maintained by mL38, which intertwines with the proteins of the base of the central protuberance and anchors the central protuberance to the rRNA core of the LSU body (Fig. 3), thereby performing a similar role to 5*S* rRNA in cytoplasmic ribosomes. ICT1 and long helical elements of mL52 and CRIF1 (Fig. 3 and fig. S15) further connect the globular domain of mL38 to the main body. A structurally similar feature of an α-helix bridging the body and central protuberance is seen in the yeast mitoribosome (*8*).

Remodeling of tRNA binding sites

Conventional tRNAs have four-armed cloverleaf secondary structures and L-shaped tertiary structures. However, many human mt-tRNAs have absent or reduced D- and/or T-loops that form the tRNA elbow (Fig. 4A) (*23*). To accommodate these highly variable loops the tRNA-binding sites have dispensed with elements, common to other ribosomes that interact with the tRNA elbow (Fig. 4B). In the A site, uL25 and the tip of h38 that are responsible for fixing the elbow of A-site tRNA in bacteria (*24*, *25*) have been lost. uL25 is also absent in the yeast mitoribosome (*8*). Similar deletions are observed in the P site, with the loss of the elbow-stabilizing uL5 and h84 (Fig. 4C). The L1 stalk, which controls the dynamics of tRNA ejection (*26*), also lacks the RNA segments (h76–h77) that bind the elbow of E-site tRNAs (*27*) (*28*)(figs. S8 and S9), although the remodeled stalk is not resolved in our structure. There do not appear to be additional stabilizing interactions at the acceptor stem, suggesting that human mt-tRNAs are less tightly bound to mitoribosomes.

The L7/L12 stalk

The L7/L12 stalk is a large ribosomal protrusion responsible for the recruitment of translation factors, as well as stimulation of factor-dependent GTP hydrolysis. In bacteria it is formed by 23*S* rRNA (h42-h44), uL10, uL11 and multiple copies of uL12 (*29*). In the absence of translational factors, the stalk is generally highly flexible and not well resolved in cryo-EM or crystal structures. In our reconstruction, the stalk is partially resolved (fig. S3B), allowing us to place homology models of uL10 and uL11. The stalk protein-binding platform (h43-h44) is also resolved despite h42, which connects the platform to the main body of the ribosome, being remodeled and flexible.

The increased stability of the L7/L12 stalk is the product of an inter-protein network not observed in other ribosomes (Fig. 5A). First, a mitochondria-specific stalk protein, mL53, bridges uL10 on the top of the stalk with bS18a in the body. The interaction between mL53 and bS18a is mediated through a shared β-sheet (Fig. 5B). Secondly, a mitochondria-specific N-terminal extension of uL10 forms a stable interaction with the main body of the mitoribosome, notably through a shared zinc-binding motif with S18a (Fig. 5C), and further coordinated by a C-terminal extension of uL16, mL63 and the loop of h39 (Fig. 5D). A linker region between the N-terminal extension and the conserved part of uL10 is not fully resolved in the maps suggesting some conformational flexibility is maintained. The differences in the L7/L12 stalk may ex-

plain why bacterial EF-G is incompatible with mammalian mitoribosomes (*30*). Additionally, uL6, which interacts with translational factors in bacteria, is not functionally replaced in the human mt-LSU (fig. S16).

The exit tunnel

The exit tunnel, through which nascent peptides pass before emerging from the ribosome, appears to be adapted for translating hydrophobic membrane proteins. Density for an endogenous polypeptide, or mixture of polypeptides, is seen throughout the exit tunnel and shows clear interactions with hydrophobic residues of the mitoribosomal tunnel wall, mainly from uL22 (Fig. 6A). These residues make the tunnel more hydrophobic than in cytoplasmic ribosomes (*13*). The hydrophobic nature of both the translated polypeptide and the exit tunnel may explain why a polypeptide remains trapped in the exit tunnel despite the lack of a P-site tRNA to tether it in the ribosome. Although the nascent peptide is better resolved in the upper part of the tunnel, broken density consistent with a helical structure is apparent closer to the exit. Thus helices of mitochondrial OXPHOS proteins may start forming within the mitoribosomal tunnel similar to what has been seen in cytoplasmic ribosomes (*13*), and the hydrophobic nature of the wall may aid this by mimicking the hydrophobic environment of the membrane that is the eventual site of these proteins. In addition, the increased hydrophobic interactions could act to slow the rate of elongation, allowing more time for transmembrane domains to fold and for assembly of OXPHOS complexes.

The presence of a nascent polypeptide also unambiguously delineates the overall tunnel path, which is similar to that of bacterial and cytoplasmic ribosomes (Fig. 6B) and different from the yeast mitoribosome (*8*). The alternative exit tunnel observed in yeast results from deletion of rRNA h16-20 and h24 (fig. S17). Despite similar deletions in domain I of the human mitoribosome, a short segment that replaces h24 (nucleotides 1806-1813) seals this potential exit and precludes a yeast-like tunnel path being formed in human mitoribosomes (fig. S17). The peptidyl transfer center and upper tunnel of the human mt-LSU are architecturally similar to bacterial ribosomes, and do not show the constriction observed in yeast (*8*).

The exit site of the mitoribosomal tunnel, where the nascent chain emerges, has two roles: forming a docking platform for maturation factors and tethering mitoribosomes to the inner mitochondrial membrane. In the human mt-LSU, this region is remodeled, with two rRNA deletions (h7 and h24) compensated by extensions and conformational changes of the conserved proteins that line the tunnel walls (Fig. 6, B to D). Deletion of h24 has caused a positional change of a β-hairpin of uL24, which exposes uL22 to the exit site, and h7 is partially replaced by uL29 and an N-terminal extension of uL24. Together these changes result in a more proteinaceous exit site than in other ribosomes and allows binding of mL45 that likely anchors the mitoribosome to the inner mitochondrial membrane in a way that would expose the translated nascent polypeptide to solvent (*9*), making it accessible to specific maturation factors and chaperones involved in the assembly of OXPHOS complexes.

Mitoribosomal mutations have been linked with hereditary mitochondrial diseases (*4*). These mutations and their potential effect on the structure are shown in tables S4 and S5 and fig. S18. Although all these mutations affect the mitoribosome, their effects are varied, suggesting that in each case they work in conjunction with other mutations to produce the disease. The structural information presented here can be used for the rational design of antibiotics with decreased autotoxicity. In addition, since mitoribosomes are involved in redirection of energy metabolism of tumorogenic cells (*31*), with many mitoribosomal proteins upregulated in cancer (table S6), the structure might be useful for the development of novel cancer therapeutics.

References and Notes

1. T. W. O'Brien, Properties of human mitochondrial ribosomes. *IUBMB Life* **55**, 505–513 (2003). Medline doi:10.1080/15216540310001626610
2. M. Liu, L. Spremulli, Interaction of mammalian mitochondrial ribosomes with the inner membrane. *J. Biol. Chem.* **275**, 29400–29406 (2000). Medline doi:10.1074/jbc.M002173200
3. D. Skladal, J. Halliday, D. R. Thorburn, Minimum birth prevalence of mitochondrial respiratory chain disorders in children. *Brain* **126**, 1905–1912 (2003). Medline doi:10.1093/brain/awg170
4. V. Boczonadi, R. Horvath, Mitochondria: Impaired mitochondrial translation in human disease. *Int. J. Biochem. Cell Biol.* **48**, 77–84 (2014). Medline doi:10.1016/j.biocel.2013.12.011
5. F. Sotgia, D. Whitaker-Menezes, U. E. Martinez-Outschoorn, A. F. Salem, A. Tsirigos, R. Lamb, S. Sneddon, J. Hulit, A. Howell, M. P. Lisanti, Mitochondria "fuel" breast cancer metabolism: Fifteen markers of mitochondrial biogenesis label epithelial cancer cells, but are excluded from adjacent stromal cells. *Cell Cycle* **11**, 4390–4401 (2012). Medline doi:10.4161/cc.22777
6. M. Skrtić, S. Sriskanthadevan, B. Jhas, M. Gebbia, X. Wang, Z. Wang, R. Hurren, Y. Jitkova, M. Gronda, N. Maclean, C. K. Lai, Y. Eberhard, J. Bartoszko, P. Spagnuolo, A. C. Rutledge, A. Datti, T. Ketela, J. Moffat, B. H. Robinson, J. H. Cameron, J. Wrana, C. J. Eaves, M. D. Minden, J. C. Wang, J. E. Dick, K. Humphries, C. Nislow, G. Giaever, A. D. Schimmer, Inhibition of mitochondrial translation as a therapeutic strategy for human acute myeloid leukemia. *Cancer Cell* **20**, 674–688 (2011). Medline doi:10.1016/j.ccr.2011.10.015
7. R. Singh, L. Sripada, R. Singh, Side effects of antibiotics during bacterial infection: Mitochondria, the main target in host cell. *Mitochondrion* **16**, 50–54 (2014). Medline doi:10.1016/j.mito.2013.10.005
8. A. Amunts, A. Brown, X. C. Bai, J. L. Llácer, T. Hussain, P. Emsley, F. Long, G. Murshudov, S. H. Scheres, V. Ramakrishnan, Structure of the yeast mitochondrial large ribosomal subunit. *Science* **343**, 1485–1489 (2014). Medline doi:10.1126/science.1249410
9. B. J. Greber, D. Boehringer, A. Leitner, P. Bieri, F. Voigts-Hoffmann, J. P. Erzberger, M. Leibundgut, R. Aebersold, N. Ban, Architecture of the large subunit of the mammalian mitochondrial ribosome. *Nature* **505**, 515–519 (2014). Medline doi:10.1038/nature12890
10. P. S. Kaushal, M. R. Sharma, T. M. Booth, E. M. Haque, C. S. Tung, K. Y. Sanbonmatsu, L. L. Spremulli, R. K. Agrawal, Cryo-EM structure of the small subunit of the mammalian mitochondrial ribosome. *Proc. Natl. Acad. Sci. U.S.A.* **111**, 7284–7289 (2014). Medline doi:10.1073/pnas.1401657111
11. Materials and methods are available as supplementary materials on *Science* Online.
12. S. H. W. Scheres, RELION: Implementation of a Bayesian approach to cryo-EM structure determination. *J. Struct. Biol.* **180**, 519–530 (2012). Medline doi:10.1016/j.jsb.2012.09.006
13. R. M. Voorhees, I. S. Fernández, S. H. W. Scheres, R. S. Hegde, Structure of the mammalian ribosome-Sec61 complex to 3.4 Å resolution. *Cell* **157**, 1632–1643 (2014). Medline doi:10.1016/j.cell.2014.05.024
14. R. N. Lightowlers, A. Rozanska, Z. M. Chrzanowska-Lightowlers, Mitochondrial protein synthesis: Figuring the fundamentals, complexities and complications, of mammalian mitochondrial translation. *FEBS Lett.* **588**, 2496–2503 (2014). Medline doi:10.1016/j.febslet.2014.05.054
15. E. C. Koc, A. Ranasinghe, W. Burkhart, K. Blackburn, H. Koc, A. Moseley, L. L. Spremulli, A new face on apoptosis: Death-associated protein 3 and PDCD9 are mitochondrial ribosomal proteins. *FEBS Lett.* **492**, 166–170 (2001). Medline doi:10.1016/S0014-5793(01)02250-5
16. E. C. Koc, W. Burkhart, K. Blackburn, A. Moseley, L. L. Spremulli, The small subunit of the mammalian mitochondrial ribosome. Identification of the full complement of ribosomal proteins present. *J. Biol. Chem.* **276**, 19363–19374 (2001). Medline
17. S. Anderson, A. T. Bankier, B. G. Barrell, M. H. de Bruijn, A. R. Coulson, J. Drouin, I. C. Eperon, D. P. Nierlich, B. A. Roe, F. Sanger, P. H. Schreier, A. J. Smith, R. Staden, I. G. Young, Sequence and organization of the human mitochondrial genome. *Nature* **290**, 457–465 (1981). Medline doi:10.1038/290457a0
18. J. Montoya, G. L. Gaines, G. Attardi, The pattern of transcription of the human mitochondrial rRNA genes reveals two overlapping transcription units. *Cell* **34**, 151–159 (1983). Medline doi:10.1016/0092-8674(83)90145-9

19. D. Liao, Gene conversion drives within genic sequences: Concerted evolution of ribosomal RNA genes in bacteria and archaea. *J. Mol. Evol.* **51**, 305–317 (2000). Medline
20. P. D'Onorio de Meo, M. D'Antonio, F. Griggio, R. Lupi, M. Borsani, G. Pavesi, T. Castrignano, G. Pesole, C. Gissi, MitoZoa 2.0: A database resource and search tools for comparative and evolutionary analyses of mitochondrial genomes in Metazoa. *Nucleic Acids Res.* **40**, D1168–D1172 (2012). Medline doi:10.1093/nar/gkr1144
21. M. H. Rhodin, R. Rakauskaitė, J. D. Dinman, The central core region of yeast ribosomal protein L11 is important for subunit joining and translational fidelity. *Mol. Genet. Genomics* **285**, 505–516 (2011). Medline doi:10.1007/s00438-011-0623-2
22. J. Noeske, J. H. D. Cate, Structural basis for protein synthesis: Snapshots of the ribosome in motion. *Curr. Opin. Struct. Biol.* **22**, 743–749 (2012). Medline doi:10.1016/j.sbi.2012.07.011
23. M. Helm, H. Brulé, D. Friede, R. Giegé, D. Pütz, C. Florentz, Search for characteristic structural features of mammalian mitochondrial tRNAs. *RNA* **6**, 1356–1379 (2000). Medline doi:10.1017/S1355838200001047
24. R. M. Voorhees, A. Weixlbaumer, D. Loakes, A. C. Kelley, V. Ramakrishnan, Insights into substrate stabilization from snapshots of the peptidyl transferase center of the intact 70S ribosome. *Nat. Struct. Mol. Biol.* **16**, 528–533 (2009). Medline doi:10.1038/nsmb.1577
25. L. Jenner, N. Demeshkina, G. Yusupova, M. Yusupov, Structural rearrangements of the ribosome at the tRNA proofreading step. *Nat. Struct. Mol. Biol.* **17**, 1072–1078 (2010). Medline doi:10.1038/nsmb.1880
26. J. Fei, J. E. Bronson, J. M. Hofman, R. L. Srinivas, C. H. Wiggins, R. L. Gonzalez Jr., Allosteric collaboration between elongation factor G and the ribosomal L1 stalk directs tRNA movements during translation. *Proc. Natl. Acad. Sci. U.S.A.* **106**, 15702–15707 (2009). Medline doi:10.1073/pnas.0908077106
27. M. R. Sharma, E. C. Koc, P. P. Datta, T. M. Booth, L. L. Spremulli, R. K. Agrawal, Structure of the mammalian mitochondrial ribosome reveals an expanded functional role for its component proteins. *Cell* **115**, 97–108 (2003). Medline doi:10.1016/S0092-8674(03)00762-1
28. J. Lehmann, F. Jossinet, D. Gautheret, A universal RNA structural motif docking the elbow of tRNA in the ribosome, RNAse P and T-box leaders. *Nucleic Acids Res.* **41**, 5494–5502 (2013). Medline doi:10.1093/nar/gkt219
29. J. M. Kavran, T. A. Steitz, Structure of the base of the L7/L12 stalk of the Haloarcula marismortui large ribosomal subunit: Analysis of L11 movements. *J. Mol. Biol.* **371**, 1047–1059 (2007). Medline doi:10.1016/j.jmb.2007.05.091
30. H. K. Chung, L. L. Spremulli, Purification and characterization of elongation factor G from bovine liver mitochondria. *J. Biol. Chem.* **265**, 21000–21004 (1990). Medline
31. D. Hanahan, R. A. Weinberg, Hallmarks of cancer: The next generation. *Cell* **144**, 646–674 (2011). Medline doi:10.1016/j.cell.2011.02.013
32. P. J. Reeves, N. Callewaert, R. Contreras, H. G. Khorana, Structure and function in rhodopsin: High-level expression of rhodopsin with restricted and homogeneous N-glycosylation by a tetracycline-inducible N-acetylglucosaminyltransferase I-negative HEK293S stable mammalian cell line. *Proc. Natl. Acad. Sci. U.S.A.* **99**, 13419–13424 (2002). Medline doi:10.1073/pnas.212519299
33. FASTX-Toolkit, http://hannonlab.cshl.edu/fastx_toolkit/
34. P. Flicek, M. R. Amode, D. Barrell, K. Beal, S. Brent, D. Carvalho-Silva, P. Clapham, G. Coates, S. Fairley, S. Fitzgerald, L. Gil, L. Gordon, M. Hendrix, T. Hourlier, N. Johnson, A. K. Kähäri, D. Keefe, S. Keenan, R. Kinsella, M. Komorowska, G. Koscielny, E. Kulesha, P. Larsson, I. Longden, W. McLaren, M. Muffato, B. Overduin, M. Pignatelli, B. Pritchard, H. S. Riat, G. R. Ritchie, M. Ruffier, M. Schuster, D. Sobral, Y. A. Tang, K. Taylor, S. Trevanion, J. Vandrovcova, S. White, M. Wilson, S. P. Wilder, B. L. Aken, E. Birney, F. Cunningham, I. Dunham, R. Durbin, X. M. Fernández-Suarez, J. Harrow, J. Herrero, T. J. Hubbard, A. Parker, G. Proctor, G. Spudich, J. Vogel, A. Yates, A. Zadissa, S. M. Searle, Ensembl 2012. *Nucleic Acids Res.* **40**, D84–D90 (2011). Medline
35. B. Langmead, C. Trapnell, M. Pop, S. L. Salzberg, Ultrafast and memory-efficient alignment of short DNA sequences to the human genome. *Genome Biol.* **10**, R25 (2009). Medline doi:10.1186/gb-2009-10-3-r25
36. F. Jühling, M. Mörl, R. K. Hartmann, M. Sprinzl, P. F. Stadler, J. Pütz, tRNAdb 2009: Compilation of tRNA sequences and tRNA genes. *Nucleic Acids Res.* **37** (Database), D159–D162 (2009). Medline doi:10.1093/nar/gkn772
37. X.-C. Bai, I. S. Fernandez, G. McMullan, S. H. Scheres, Ribosome structures to near-atomic resolution from thirty thousand cryo-EM particles. *eLife* **2**, e00461 (2013). Medline doi:10.7554/eLife.00461
38. G. Tang, L. Peng, P. R. Baldwin, D. S. Mann, W. Jiang, I. Rees, S. J. Ludtke, EMAN2: An extensible image processing suite for electron microscopy. *J. Struct. Biol.* **157**, 38–46 (2007). Medline doi:10.1016/j.jsb.2006.05.009
39. J. A. Mindell, N. Grigorieff, Accurate determination of local defocus and specimen tilt in electron microscopy. *J. Struct. Biol.* **142**, 334–347 (2003). Medline doi:10.1016/S1047-8477(03)00069-8
40. S. H. Scheres, Beam-induced motion correction for sub-megadalton cryo-EM particles. *eLife* **3**, e03665 (2014). Medline doi:10.7554/eLife.03665
41. A. Kucukelbir, F. J. Sigworth, H. D. Tagare, Quantifying the local resolution of cryo-EM density maps. *Nat. Methods* **11**, 63–65 (2014). Medline doi:10.1038/nmeth.2727
42. S. H. W. Scheres, S. Chen, Prevention of overfitting in cryo-EM structure determination. *Nat. Methods* **9**, 853–854 (2012). Medline doi:10.1038/nmeth.2115
43. S. Chen, G. McMullan, A. R. Faruqi, G. N. Murshudov, J. M. Short, S. H. Scheres, R. Henderson, High-resolution noise substitution to measure overfitting and validate resolution in 3D structure determination by single particle electron cryomicroscopy. *Ultramicroscopy* **135**, 24–35 (2013). Medline doi:10.1016/j.ultramic.2013.06.004
44. P. B. Rosenthal, R. Henderson, Optimal determination of particle orientation, absolute hand, and contrast loss in single-particle electron cryomicroscopy. *J. Mol. Biol.* **333**, 721–745 (2003). Medline doi:10.1016/j.jmb.2003.07.013
45. R. M. Andrews, I. Kubacka, P. F. Chinnery, R. N. Lightowlers, D. M. Turnbull, N. Howell, Reanalysis and revision of the Cambridge reference sequence for human mitochondrial DNA. *Nat. Genet.* **23**, 147 (1999). Medline doi:10.1038/13779
46. N. Ban, R. Beckmann, J. H. Cate, J. D. Dinman, F. Dragon, S. R. Ellis, D. L. Lafontaine, L. Lindahl, A. Liljas, J. M. Lipton, M. A. McAlear, P. B. Moore, H. F. Noller, J. Ortega, V. G. Panse, V. Ramakrishnan, C. M. Spahn, T. A. Steitz, M. Tchorzewski, D. Tollervey, A. J. Warren, J. R. Williamson, D. Wilson, A. Yonath, M. Yusupov, A new system for naming ribosomal proteins. *Curr. Opin. Struct. Biol.* **24**, 165–169 (2014). Medline doi:10.1016/j.sbi.2014.01.002
47. P. Maly, R. Brimacombe, Refined secondary structure models for the 16S and 23S ribosomal RNA of *Escherichia coli*. *Nucleic Acids Res.* **11**, 7263–7286 (1983). Medline doi:10.1093/nar/11.21.7263
48. E. F. Pettersen, T. D. Goddard, C. C. Huang, G. S. Couch, D. M. Greenblatt, E. C. Meng, T. E. Ferrin, UCSF Chimera: A visualization system for exploratory research and analysis. *J. Comput. Chem.* **25**, 1605–1612 (2004). Medline doi:10.1002/jcc.20084
49. UniProt Consortium, Update on activities at the Universal Protein Resource (UniProt) in 2013. *Nucleic Acids Res.* **41** (D1), D43–D47 (2013). Medline doi:10.1093/nar/gks1068
50. F. Sievers, A. Wilm, D. Dineen, T. J. Gibson, K. Karplus, W. Li, R. Lopez, H. McWilliam, M. Remmert, J. Söding, J. D. Thompson, D. G. Higgins, Fast, scalable generation of high-quality protein multiple sequence alignments using Clustal Omega. *Mol. Syst. Biol.* **7**, 539 (2011). Medline doi:10.1038/msb.2011.75
51. P. Emsley, B. Lohkamp, W. G. Scott, K. Cowtan, Features and development of Coot. *Acta Crystallogr. D Biol. Crystallogr.* **66**, 486–501 (2010). Medline doi:10.1107/S0907444910007493
52. D. S. Tourigny, I. S. Fernández, A. C. Kelley, V. Ramakrishnan, Elongation factor G bound to the ribosome in an intermediate state of translocation. *Science* **340**, 1235490 (2013). Medline doi:10.1126/science.1235490
53. G. N. Murshudov, P. Skubák, A. A. Lebedev, N. S. Pannu, R. A. Steiner, R. A. Nicholls, M. D. Winn, F. Long, A. A. Vagin, REFMAC5 for the refinement of macromolecular crystal structures. *Acta Crystallogr. D Biol. Crystallogr.* **67**, 355–367 (2011). Medline doi:10.1107/S0907444911001314
54. R. A. Nicholls, F. Long, G. N. Murshudov, Low-resolution refinement tools in REFMAC5. *Acta Crystallogr. D Biol. Crystallogr.* **68**, 404–417 (2012). Medline doi:10.1107/S090744491105606X
55. V. B. Chen, W. B. Arendall 3rd, J. J. Headd, D. A. Keedy, R. M. Immormino, G. J. Kapral, L. W. Murray, J. S. Richardson, D. C. Richardson, MolProbity: All-atom structure validation for macromolecular crystallography. *Acta Crystallogr. D Biol. Crystallogr.* **66**, 12–21 (2010). Medline

doi:10.1107/S0907444909042073
56. I. S. Fernández, X.-C. Bai, G. Murshudov, S. H. W. Scheres, V. Ramakrishnan, Initiation of translation by cricket paralysis virus IRES requires its translocation in the ribosome. *Cell* **157**, 823–831 (2014). Medline doi:10.1016/j.cell.2014.04.015
57. P. Shannon, A. Markiel, O. Ozier, N. S. Baliga, J. T. Wang, D. Ramage, N. Amin, B. Schwikowski, T. Ideker, Cytoscape: A software environment for integrated models of biomolecular interaction networks. *Genome Res.* **13**, 2498–2504 (2003). Medline doi:10.1101/gr.1239303
58. E. Krissinel, K. Henrick, Inference of macromolecular assemblies from crystalline state. *J. Mol. Biol.* **372**, 774–797 (2007). Medline doi:10.1016/j.jmb.2007.05.022
59. B. K. Ho, F. Gruswitz, HOLLOW: Generating accurate representations of channel and interior surfaces in molecular structures. *BMC Struct. Biol.* **8**, 49 (2008). Medline doi:10.1186/1472-6807-8-49
60. W. L. DeLano, The PyMOL molecular graphics system (2002).
61. X.-J. Lu, W. K. Olson, 3DNA: A versatile, integrated software system for the analysis, rebuilding and visualization of three-dimensional nucleic-acid structures. *Nat. Protoc.* **3**, 1213–1227 (2008). Medline doi:10.1038/nprot.2008.104
62. K. Darty, A. Denise, Y. Ponty, VARNA: Interactive drawing and editing of the RNA secondary structure. *Bioinformatics* **25**, 1974–1975 (2009). Medline doi:10.1093/bioinformatics/btp250
63. E. Krissinel, K. Henrick, Secondary-structure matching (SSM), a new tool for fast protein structure alignment in three dimensions. *Acta Crystallogr. D Biol. Crystallogr.* **60**, 2256–2268 (2004). Medline doi:10.1107/S0907444904026460
64. L. Holm, P. Rosenström, Dali server: Conservation mapping in 3D. *Nucleic Acids Res.* **38**, W545–W549 (2010). Medline doi:10.1093/nar/gkq366
65. Y. V. Surovtseva, T. E. Shutt, J. Cotney, H. Cimen, S. Y. Chen, E. C. Koc, G. S. Shadel, Mitochondrial ribosomal protein L12 selectively associates with human mitochondrial RNA polymerase to activate transcription. *Proc. Natl. Acad. Sci. U.S.A.* **108**, 17921–17926 (2011). Medline doi:10.1073/pnas.1108852108
66. Y. A. Yoo, M. J. Kim, J. K. Park, Y. M. Chung, J. H. Lee, S. G. Chi, J. S. Kim, Y. D. Yoo, Mitochondrial ribosomal protein L41 suppresses cell growth in association with p53 and p27Kip1. *Mol. Cell. Biol.* **25**, 6603–6616 (2005). Medline doi:10.1128/MCB.25.15.6603-6616.2005
67. J. A. Conde, C. J. Claunch, H. E. Romo, A. Benito-Martín, R. P. Ballestero, M. González-García, Identification of a motif in BMRP required for interaction with Bcl-2 by site-directed mutagenesis studies. *J. Cell. Biochem.* **113**, 3498–3508 (2012). Medline doi:10.1002/jcb.24226
68. E. C. Koc, W. Burkhart, K. Blackburn, M. B. Moyer, D. M. Schlatzer, A. Moseley, L. L. Spremulli, The large subunit of the mammalian mitochondrial ribosome. Analysis of the complement of ribosomal proteins present. *J. Biol. Chem.* **276**, 43958–43969 (2001). Medline doi:10.1074/jbc.M106510200
69. Z. Polianskyte, N. Peitsaro, A. Dapkunas, J. Liobikas, R. Soliymani, M. Lalowski, O. Speer, J. Seitsonen, S. Butcher, G. M. Cereghetti, M. D. Linder, M. Merckel, J. Thompson, O. Eriksson, LACTB is a filament-forming protein localized in mitochondria. *Proc. Natl. Acad. Sci. U.S.A.* **106**, 18960–18965 (2009). Medline doi:10.1073/pnas.0906734106
70. H. J. Kang, Y. B. Hong, H. J. Kim, I. Bae, CR6-interacting factor 1 (CRIF1) regulates NF-E2-related factor 2 (NRF2) protein stability by proteasome-mediated degradation. *J. Biol. Chem.* **285**, 21258–21268 (2010). Medline doi:10.1074/jbc.M109.084590
71. J. H. Suh, M. Shong, H. S. Choi, K. Lee, CR6-interacting factor 1 represses the transactivation of androgen receptor by direct interaction. *Mol. Endocrinol.* **22**, 33–46 (2008). Medline doi:10.1210/me.2007-0194
72. M. C. Kwon, B. K. Koo, J. S. Moon, Y. Y. Kim, K. C. Park, N. S. Kim, M. Y. Kwon, M. P. Kong, K. J. Yoon, S. K. Im, J. Ghim, Y. M. Han, S. K. Jang, M. Shong, Y. Y. Kong, Crif1 is a novel transcriptional coactivator of STAT3. *EMBO J.* **27**, 642–653 (2008). Medline doi:10.1038/sj.emboj.7601986
73. H. K. Chung, Y. W. Yi, N. C. Jung, D. Kim, J. M. Suh, H. Kim, K. C. Park, J. H. Song, D. W. Kim, E. S. Hwang, S. H. Yoon, Y. S. Bae, J. M. Kim, I. Bae, M. Shong, CR6-interacting factor 1 interacts with Gadd45 family proteins and modulates the cell cycle. *J. Biol. Chem.* **278**, 28079–28088 (2003). Medline doi:10.1074/jbc.M212835200
74. M. C. Kwon, B. K. Koo, Y. Y. Kim, S. H. Lee, N. S. Kim, J. H. Kim, Y. Y. Kong, Essential role of CR6-interacting factor 1 (Crif1) in E74-like factor 3 (ELF3)-mediated intestinal development. *J. Biol. Chem.* **284**, 33634–33641 (2009). Medline doi:10.1074/jbc.M109.059840
75. MITOMAP: A human mitochondrial genome database. http://www.mitomap.org (2013).
76. V. Tiranti, L. D'Agruma, D. Pareyson, M. Mora, F. Carrara, L. Zelante, P. Gasparini, M. Zeviani, A novel mutation in the mitochondrial tRNA(Val) gene associated with a complex neurological presentation. *Ann. Neurol.* **43**, 98–101 (1998). Medline doi:10.1002/ana.410430116
77. S. Sacconi, L. Salviati, C. Gooch, E. Bonilla, S. Shanske, S. DiMauro, Complex neurologic syndrome associated with the G1606A mutation of mitochondrial DNA. *Arch. Neurol.* **59**, 1013–1015 (2002). Medline doi:10.1001/archneur.59.6.1013
78. R. McFarland, K. M. Clark, A. A. Morris, R. W. Taylor, S. Macphail, R. N. Lightowlers, D. M. Turnbull, Multiple neonatal deaths due to a homoplasmic mitochondrial DNA mutation. *Nat. Genet.* **30**, 145–146 (2002). Medline doi:10.1038/ng819
79. A. M. Schaefer, R. McFarland, E. L. Blakely, L. He, R. G. Whittaker, R. W. Taylor, P. F. Chinnery, D. M. Turnbull, Prevalence of mitochondrial DNA disease in adults. *Ann. Neurol.* **63**, 35–39 (2008). Medline doi:10.1002/ana.21217
80. J. J. Arredondo, M. E. Gallardo, P. García-Pavía, V. Domingo, B. Bretón, M. T. García-Silva, M. J. Sedano, M. A. Martín, J. Arenas, M. Cervera, R. Garesse, B. Bornstein, Mitochondrial tRNA valine as a recurrent target for mutations involved in mitochondrial cardiomyopathies. *Mitochondrion* **12**, 357–362 (2012). Medline doi:10.1016/j.mito.2011.09.010
81. R. Horváth, A. Bender, A. Abicht, E. Holinski-Feder, B. Czermin, T. Trips, P. Schneiderat, H. Lochmüller, T. Klopstock, Heteroplasmic mutation in the anticodon-stem of mitochondrial tRNA(Val) causing MNGIE-like gastrointestinal dysmotility and cachexia. *J. Neurol.* **256**, 810–815 (2009). Medline doi:10.1007/s00415-009-5023-8
82. C. Glatz, K. D'Aco, S. Smith, N. Sondheimer, Mutation in the mitochondrial tRNAVal causes mitochondrial encephalopathy, lactic acidosis and stroke-like episodes. *Mitochondrion* **11**, 615–619 (2011). Medline doi:10.1016/j.mito.2011.04.003
83. I. F. de Coo, E. A. Sistermans, I. J. de Wijs, C. Catsman-Berrevoets, H. F. Busch, H. R. Scholte, J. B. de Klerk, B. A. van Oost, H. J. Smeets, A mitochondrial tRNA(Val) gene mutation (G1642A) in a patient with mitochondrial myopathy, lactic acidosis, and stroke-like episodes. *Neurology* **50**, 293–295 (1998). Medline doi:10.1212/WNL.50.1.293
84. R. W. Taylor, P. F. Chinnery, F. Haldane, A. A. Morris, L. A. Bindoff, D. M. Turnbull, J. Wilson, MELAS associated with a mutation in the valine transfer RNA gene of mitochondrial DNA. *Ann. Neurol.* **40**, 459–462 (1996). Medline doi:10.1002/ana.410400318
85. M. del Mar O'Callaghan, S. Emperador, E. López-Gallardo, C. Jou, N. Buján, R. Montero, A. Garcia-Cazorla, D. Gonzaga, I. Ferrer, P. Briones, E. Ruiz-Pesini, M. Pineda, R. Artuch, J. Montoya, New mitochondrial DNA mutations in tRNA associated with three severe encephalopamyopathic phenotypes: Neonatal, infantile, and childhood onset. *Neurogenetics* **13**, 245–250 (2012). Medline doi:10.1007/s10048-012-0322-0
86. R. M. Chalmers, P. J. Lamont, I. Nelson, D. W. Ellison, N. H. Thomas, A. E. Harding, S. R. Hammans, A mitochondrial DNA tRNA(Val) point mutation associated with adult-onset Leigh syndrome. *Neurology* **49**, 589–592 (1997). Medline doi:10.1212/WNL.49.2.589
87. N. Mostafaie, W. Rossmanith, H. Hombauer, T. Dechat, T. Raffelsberger, K. Bauer, B. Worofka, E. Kittl, J. Hofmann, M. Hejtman, W. Kirchmeyr, W. Schreiber, S. Weissgram, S. Jungwirth, P. Fischer, R. Bittner, K. Huber, Mitochondrial genotype and risk for Alzheimer's disease: Cross-sectional data from the Vienna-Transdanube-Aging "VITA" study. *J. Neural Transm.* **111**, 1155–1165 (2004). Medline doi:10.1007/s00702-004-0161-8
88. F. Menotti, A. Brega, M. Diegoli, M. Grasso, M. G. Modena, E. Arbustini, A novel mtDNA point mutation in tRNA(Val) is associated with hypertrophic cardiomyopathy and MELAS. *Ital. Heart J.* **5**, 460–465 (2004). Medline
89. K. Tanji, P. Kaufmann, A. B. Naini, J. Lu, T. C. Parsons, D. Wang, J. Z. Willey, S. Shanske, M. Hirano, E. Bonilla, A. Khandji, S. Dimauro, L. P. Rowland, A novel tRNA(Val) mitochondrial DNA mutation causing MELAS. *J. Neurol. Sci.* **270**, 23–27 (2008). Medline doi:10.1016/j.jns.2008.01.016
90. E. L. Blakely, J. Poulton, M. Pike, F. Wojnarowska, D. M. Turnbull, R. McFarland, R. W. Taylor, Childhood neurological presentation of a novel mitochondrial tRNA(Val) gene mutation. *J. Neurol. Sci.* **225**, 99–103 (2004).

Medline doi:10.1016/j.jns.2004.07.007
91. M. S. Fliss, H. Usadel, O. L. Caballero, L. Wu, M. R. Buta, S. M. Eleff, J. Jen, D. Sidransky, Facile detection of mitochondrial DNA mutations in tumors and bodily fluids. *Science* **287**, 2017–2019 (2000). Medline doi:10.1126/science.287.5460.2017
92. J. B. Jones, J. J. Song, P. M. Hempen, G. Parmigiani, R. H. Hruban, S. E. Kern, Detection of mitochondrial DNA mutations in pancreatic cancer offers a "mass"-ive advantage over detection of nuclear DNA mutations. *Cancer Res.* **61**, 1299–1304 (2001). Medline
93. Y. Nishigaki, R. Martí, W. C. Copeland, M. Hirano, Site-specific somatic mitochondrial DNA point mutations in patients with thymidine phosphorylase deficiency. *J. Clin. Invest.* **111**, 1913–1921 (2003). Medline doi:10.1172/JCI17828
94. R. W. Taylor, M. J. Barron, G. M. Borthwick, A. Gospel, P. F. Chinnery, D. C. Samuels, G. A. Taylor, S. M. Plusa, S. J. Needham, L. C. Greaves, T. B. Kirkwood, D. M. Turnbull, Mitochondrial DNA mutations in human colonic crypt stem cells. *J. Clin. Invest.* **112**, 1351–1360 (2003). Medline doi:10.1172/JCI19435
95. K. Polyak, Y. Li, H. Zhu, C. Lengauer, J. K. Willson, S. D. Markowitz, M. A. Trush, K. W. Kinzler, B. Vogelstein, Somatic mutations of the mitochondrial genome in human colorectal tumours. *Nat. Genet.* **20**, 291–293 (1998). Medline doi:10.1038/3108
96. Z. Liu, Y. Song, D. Li, X. He, S. Li, B. Wu, W. Wang, S. Gu, X. Zhu, X. Wang, Q. Zhou, Y. Dai, Q. Yan, The novel mitochondrial 16S rRNA 2336T>C mutation is associated with hypertrophic cardiomyopathy. *J. Med. Genet.* **51**, 176–184 (2014). Medline doi:10.1136/jmedgenet-2013-101818
97. S. Tang, A. Batra, Y. Zhang, E. S. Ebenroth, T. Huang, Left ventricular noncompaction is associated with mutations in the mitochondrial genome. *Mitochondrion* **10**, 350–357 (2010). Medline doi:10.1016/j.mito.2010.02.003
98. A. M. Porcelli, A. Ghelli, C. Ceccarelli, M. Lang, G. Cenacchi, M. Capristo, L. F. Pennisi, I. Morra, E. Ciccarelli, A. Melcarne, A. Bartoletti-Stella, N. Salfi, G. Tallini, A. Martinuzzi, V. Carelli, M. Attimonelli, M. Rugolo, G. Romeo, G. Gasparre, The genetic and metabolic signature of oncocytic transformation implicates HIF1alpha destabilization. *Hum. Mol. Genet.* **19**, 1019–1032 (2010). Medline doi:10.1093/hmg/ddp566
99. J. Tang, Y. Qi, X. H. Bao, X. R. Wu, Mutational analysis of mitochondrial DNA of children with Rett syndrome. *Pediatr. Neurol.* **17**, 327–330 (1997). Medline doi:10.1016/S0887-8994(97)00151-3
100. A. Bayat, J. Walter, H. Lambe, J. S. Watson, J. K. Stanley, M. Marino, M. W. Ferguson, W. E. Ollier, Identification of a novel mitochondrial mutation in Dupuytren's disease using multiplex DHPLC. *Plast. Reconstr. Surg.* **115**, 134–141 (2005). Medline
101. E. R. Anderson, J. K. Burmester, M. D. Caldwell, Evaluation of a mitochondrial DNA mutation in maternally inherited and sporadic cases of Dupuytren disease. *Clin. Med. Res.* **10**, 122–126 (2012). Medline doi:10.3121/cmr.2012.1063
102. C. Jerónimo, S. Nomoto, O. L. Caballero, H. Usadel, R. Henrique, G. Varzim, J. Oliveira, C. Lopes, M. S. Fliss, D. Sidransky, Mitochondrial mutations in early stage prostate cancer and bodily fluids. *Oncogene* **20**, 5195–5198 (2001). Medline doi:10.1038/sj.onc.1204646
103. A. Lorenc, J. Bryk, P. Golik, J. Kupryjańczyk, J. Ostrowski, M. Pronicki, A. Semczuk, M. Szołkowska, E. Bartnik, Homoplasmic MELAS A3243G mtDNA mutation in a colon cancer sample. *Mitochondrion* **3**, 119–124 (2003). Medline doi:10.1016/S1567-7249(03)00106-5
104. E. A. Zaki, T. Freilinger, T. Klopstock, E. E. Baldwin, K. R. Heisner, K. Adams, M. Dichgans, S. Wagler, R. G. Boles, Two common mitochondrial DNA polymorphisms are highly associated with migraine headache and cyclic vomiting syndrome. *Cephalalgia* **29**, 719–728 (2009). Medline doi:10.1111/j.1468-2982.2008.01793.x
105. L. Coulbault, B. Deslandes, D. Herlicoviez, M. H. Read, N. Leporrier, S. Schaeffer, A. Mouadil, A. Lombès, F. Chapon, P. Jauzac, S. Allouche, A novel mutation 3090 G>A of the mitochondrial 16S ribosomal RNA associated with myopathy. *Biochem. Biophys. Res. Commun.* **362**, 601–605 (2007). Medline doi:10.1016/j.bbrc.2007.08.040
106. R. H. Hsieh, J. Y. Li, C. Y. Pang, Y. H. Wei, A novel mutation in the mitochondrial 16S rRNA gene in a patient with MELAS syndrome, diabetes mellitus, hyperthyroidism and cardiomyopathy. *J. Biomed. Sci.* **8**, 328–335 (2001). Medline doi:10.1007/BF02258374
107. J. M. Shoffner, M. D. Brown, A. Torroni, M. T. Lott, M. F. Cabell, S. S. Mirra, M. F. Beal, C.-C. Yang, M. Gearing, R. Salvo, R. L. Watts, J. L. Juncos, L. A. Hansen, B. J. Crain, M. Fayad, C. L. Reckord, D. C. Wallace, Mitochondrial DNA variants observed in Alzheimer disease and Parkinson disease patients. *Genomics* **17**, 171–184 (1993). Medline doi:10.1006/geno.1993.1299
108. L. Galmiche, V. Serre, M. Beinat, Z. Assouline, A. S. Lebre, D. Chretien, P. Nietschke, V. Benes, N. Boddaert, D. Sidi, F. Brunelle, M. Rio, A. Munnich, A. Rötig, Exome sequencing identifies MRPL3 mutation in mitochondrial cardiomyopathy. *Hum. Mutat.* **32**, 1225–1231 (2011). Medline doi:10.1002/humu.21562
109. V. Serre, A. Rozanska, M. Beinat, D. Chretien, N. Boddaert, A. Munnich, A. Rötig, Z. M. Chrzanowska-Lightowlers, Mutations in mitochondrial ribosomal protein MRPL12 leads to growth retardation, neurological deterioration and mitochondrial translation deficiency. *Biochim. Biophys. Acta* **1832**, 1304–1312 (2013). Medline doi:10.1016/j.bbadis.2013.04.014
110. C. J. Carroll, P. Isohanni, R. Pöyhönen, L. Euro, U. Richter, V. Brilhante, A. Götz, T. Lahtinen, A. Paetau, H. Pihko, B. J. Battersby, H. Tyynismaa, A. Suomalainen, Whole-exome sequencing identifies a mutation in the mitochondrial ribosome protein MRPL44 to underlie mitochondrial infantile cardiomyopathy. *J. Med. Genet.* **50**, 151–159 (2013). Medline doi:10.1136/jmedgenet-2012-101375
111. M. Nolden, S. Ehses, M. Koppen, A. Bernacchia, E. I. Rugarli, T. Langer, The m-AAA protease defective in hereditary spastic paraplegia controls ribosome assembly in mitochondria. *Cell* **123**, 277–289 (2005). Medline doi:10.1016/j.cell.2005.08.003
112. I. Valles, M. J. Pajares, V. Segura, E. Guruceaga, J. Gomez-Roman, D. Blanco, A. Tamura, L. M. Montuenga, R. Pio, Identification of novel deregulated RNA metabolism-related genes in non-small cell lung cancer. *PLOS ONE* **7**, e42086 (2012). Medline doi:10.1371/journal.pone.0042086
113. R. Ribeiro, C. Monteiro, V. Catalán, P. Hu, V. Cunha, A. Rodríguez, J. Gómez-Ambrosi, A. Fraga, P. Príncipe, C. Lobato, F. Lobo, A. Morais, V. Silva, J. Sanches-Magalhães, J. Oliveira, F. Pina, C. Lopes, R. Medeiros, G. Frühbeck, Obesity and prostate cancer: Gene expression signature of human periprostatic adipose tissue. *BMC Med.* **10**, 108 (2012). Medline
114. J. C. Kim, S. Y. Kim, S. A. Roh, D. H. Cho, D. D. Kim, J. H. Kim, Y. S. Kim, Gene expression profiling: Canonical molecular changes and clinicopathological features in sporadic colorectal cancers. *World J. Gastroenerology* **14**, 6662–6672 (2008). Medline doi:10.3748/wjg.14.6662
115. C. J. M. Best, J. W. Gillespie, Y. Yi, G. V. Chandramouli, M. A. Perlmutter, Y. Gathright, H. S. Erickson, L. Georgevich, M. A. Tangrea, P. H. Duray, S. González, A. Velasco, W. M. Linehan, R. J. Matusik, D. K. Price, W. D. Figg, M. R. Emmert-Buck, R. F. Chuaqui, Molecular alterations in primary prostate cancer after androgen ablation therapy. *Clin. Cancer Res.* **11**, 6823–6834 (2005). Medline doi:10.1158/1078-0432.CCR-05-0585
116. X. Zhang, Q. Ran, Z. Li, Y. Liu, X. Liang, X. Chen, Cell cycle arrest of Jurkat cells by leukemic bone marrow stromal cells: Possible mechanisms and involvement of CRIF1. *Transplant. Proc.* **43**, 2770–2773 (2011). Medline doi:10.1016/j.transproceed.2011.05.048
117. C. C. Huang, S. H. Tu, H. H. Lien, J. Y. Jeng, C. S. Huang, C. J. Huang, L. C. Lai, E. Y. Chuang, Concurrent gene signatures for Han Chinese breast cancers. *PLOS ONE* **8**, e76421 (2013). Medline doi:10.1371/journal.pone.0076421
118. Y. Wang, L. Dong, H. Cui, D. H. Shen, Y. Wang, X. H. Chang, T. Y. Fu, X. Ye, Y. Y. Yao, Up-regulation of mitochondrial antioxidation signals in ovarian cancer cells with aggressive biologic behavior. *J. Zhejiang Univ. Sci. B* **12**, 346–356 (2011). Medline doi:10.1631/jzus.B1000192
119. Y.-W. Lin, P. D. Aplan, Gene expression profiling of precursor T-cell lymphoblastic leukemia/lymphoma identifies oncogenic pathways that are potential therapeutic targets. *Leukemia* **21**, 1276–1284 (2007). Medline doi:10.1038/sj.leu.2404685
120. G. Casari, M. De Fusco, S. Ciarmatori, M. Zeviani, M. Mora, P. Fernandez, G. De Michele, A. Filla, S. Cocozza, R. Marconi, A. Dürr, B. Fontaine, A. Ballabio, Spastic paraplegia and OXPHOS impairment caused by mutations in paraplegin, a nuclear-encoded mitochondrial metalloprotease. *Cell* **93**, 973–983 (1998). Medline doi:10.1016/S0092-8674(00)81203-9

Acknowledgments: We thank Y. Gordiyenko for help with rRNA purification; S. Peak-Chew and M. Skehel for mass spectrometry; G. McMullan, X. Chen, and C. Savva for help with data collection; J. Grimmett and T. Darling for help with computing; and I. S. Fernández and J. L. Llácer for stimulating

discussions. This work was funded by grants from the UK Medical Research Council (MC_U105184332 to V.R. and MC_UP_A025_1013 to S.H.W.S.); a Wellcome Trust Senior Investigator award (WT096570), the Agouron Institute and the Jeantet Foundation (V.R.); fellowships from Human Frontiers Science Program (A.A.), and EU FP7 Marie Curie (X.B.). Cryo-EM density maps have been deposited with the EMDB (accession number EMD-2762), and coordinates have been deposited with the PDB (entry code 3J7Y).

30 June 2014; accepted 23 September 2014
Published online 2 October 2014

Supplementary Materials
www.sciencemag.org/cgi/content/full/science.1258026/DC1
Materials and Methods
Figs. S1 to S18
Tables S1 to S6
References (*32–120*)
10.1126/science.1258026

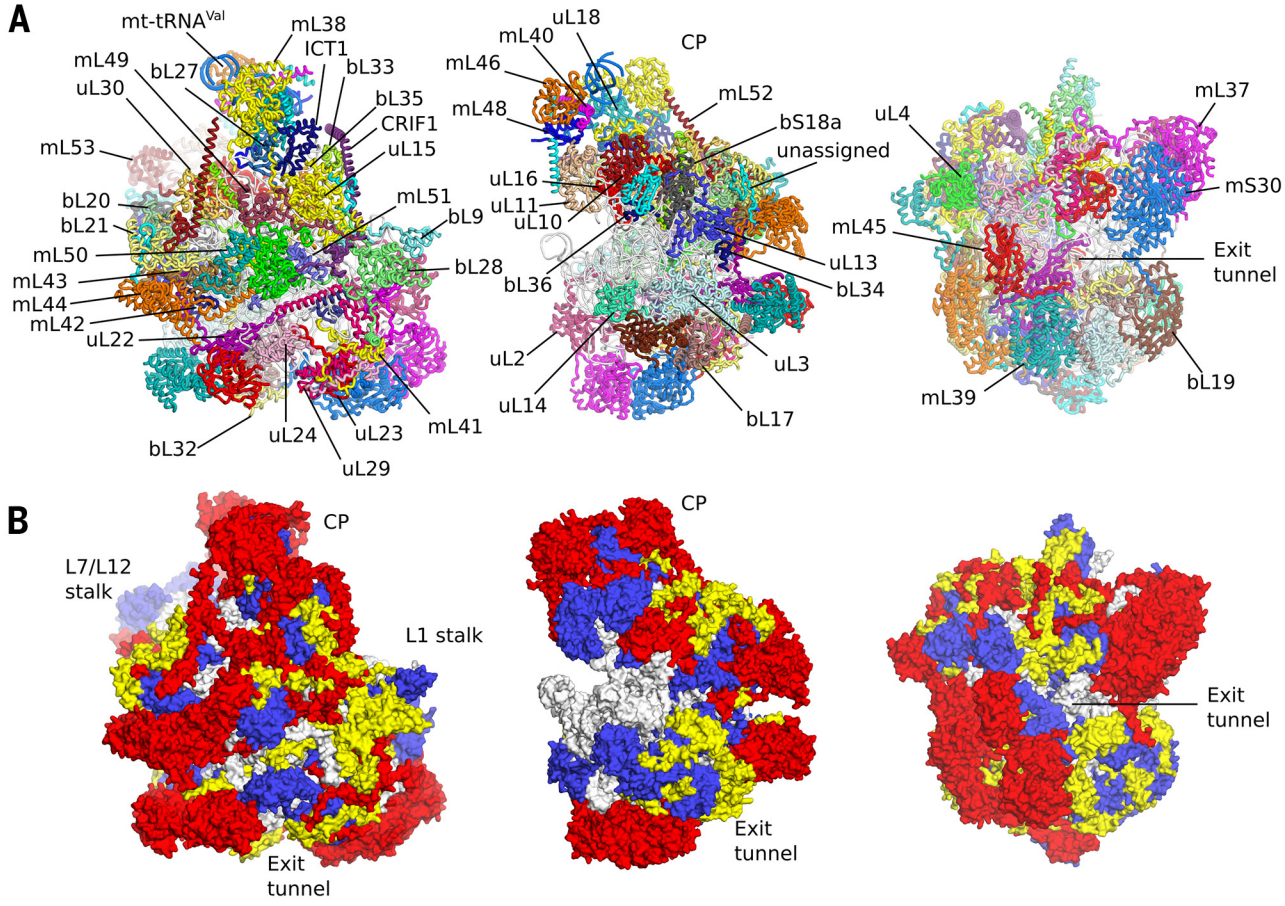

Fig. 1. Overview of human mt-LSU. (**A**) Location of proteins in the human mt-LSU, showing (from left to right) solvent-facing, side and exit tunnel views. (**B**) Views as in A, proteins conserved with bacteria (blue), extensions of homologous proteins (yellow) and mitochondria-specific proteins (red). rRNA is shown in gray.

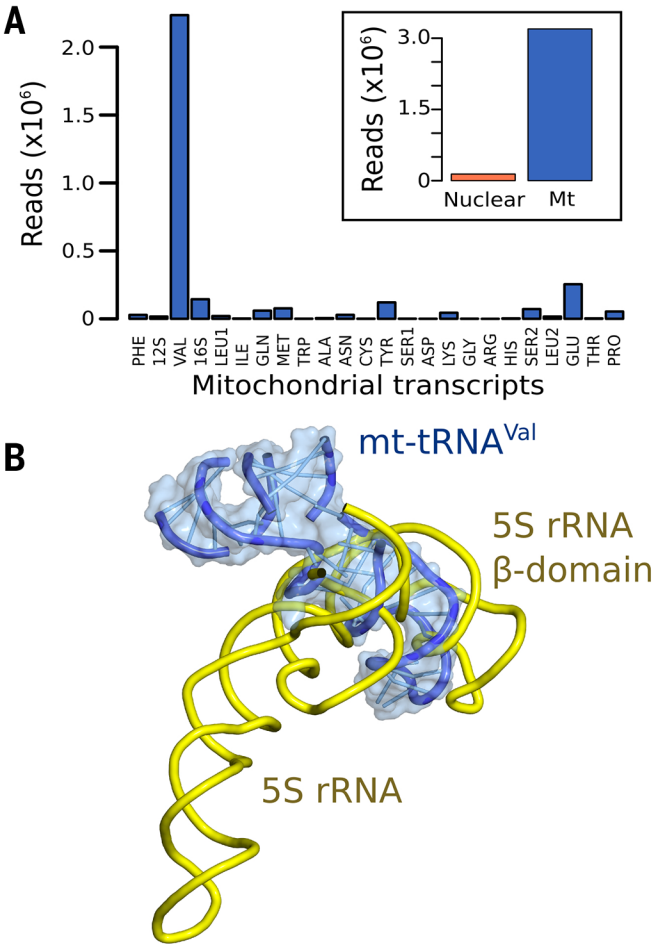

Fig. 2. Mt-tRNA^{Val} is part of the human mitoribosome. (**A**) Mapping of rRNA-sequencing reads to total human (inset) and mitochondrial transcripts. (**B**) The anticodon stem-loop of mt-tRNA^{Val} binds in a similar position to domain β of 5*S* rRNA.

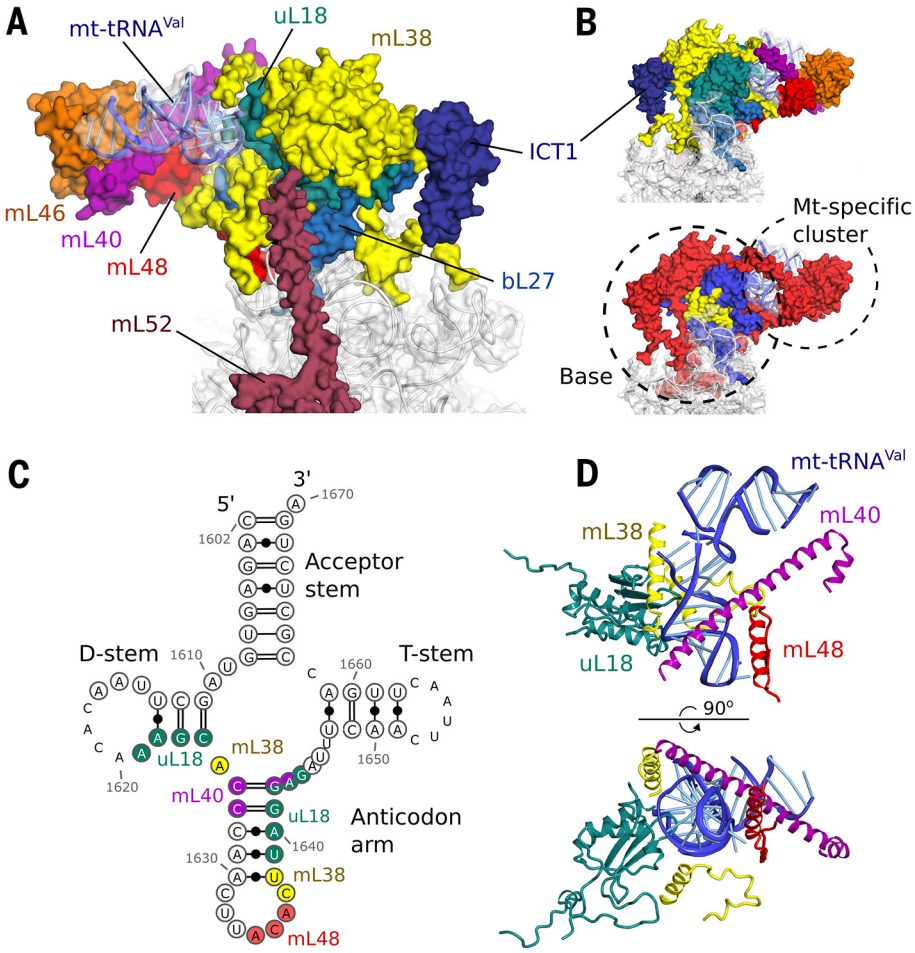

Fig. 3. The central protuberance containing mt-tRNA^{Val}. (**A**) Relative locations of proteins and mt-tRNA^{Val} in the central protuberance. (**B**). View of A rotated by 180°, colored by proteins (top) and conservation (bottom) in accordance with Fig. 1. (**C**) Secondary structure of mt-tRNA^{Val}. Modeled nucleotides are circled, and those interacting with surrounding proteins are colored. (**D**) The anticodon arm of mt-tRNA^{Val} (blue) interacts extensively with proteins, whereas the acceptor arm is solvent exposed.

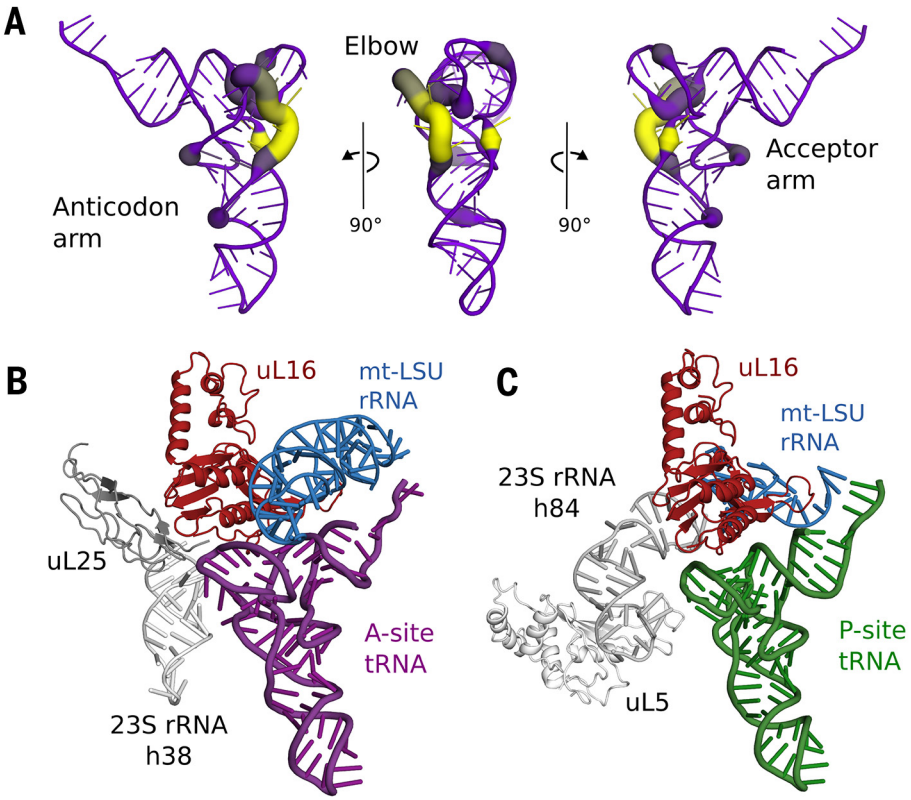

Fig. 4. Coevolution of mt-tRNAs and their binding sites. (**A**) Variability in the elbow region of human mt-tRNAs. The deletion of nucleotides relative to a bacterial tRNA (PDB ID: 2WDI) is shown by line color and thickness, with yellow and thick lines indicating most frequently deleted. (**B**) Modeling a bacterial A-site tRNA (purple) reveals that uL25 and 23*S* rRNA h38 (both gray) that stabilize the tRNA elbow region are deleted compared to bacterial ribosomes. (**C**) Similarly, uL5 and 23*S* rRNA h84 (both gray) that stabilize the elbow region of P-site tRNA (green), are deleted, but elements that bind the anticodon arm are conserved.

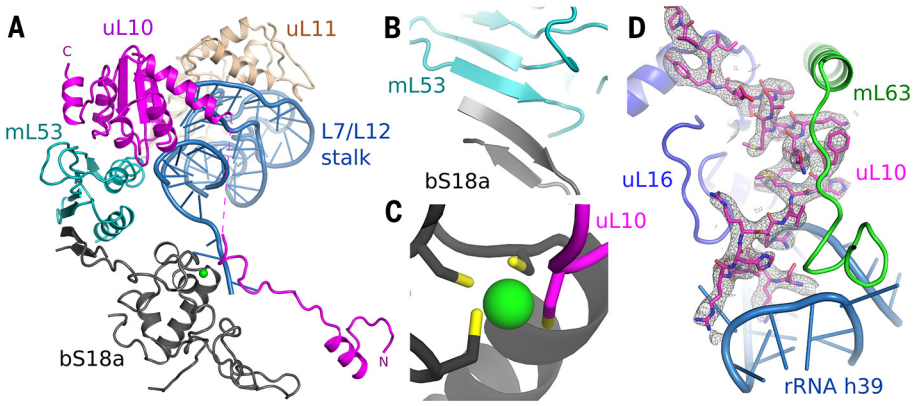

Fig. 5. Remodeling of the L7/L12 stalk. (**A**) Overview of new elements at the L7/L12 stalk. (**B**) bS18a forms a shared β-sheet with mL53 to connect the stalk to the body of the mitoribosome. (**C**) The novel N-terminal extension of uL10 contributes a cysteine residue to a shared zinc-binding motif with bS18a. (**D**) Density for the N-terminal extension of uL10 that is highly coordinated to the body of the ribosome.

Fig. 6. The exit tunnel. (**A**) Slice through the mt-LSU showing nascent chain density (cyan) in the exit tunnel. The nascent polypeptide interacts with a β-hairpin of uL22 enriched with hydrophobic residues. (**B**) The exit tunnel in bacteria (left, red) and human mitoribosomes (right, blue) showing a view of the polypeptide exit site below. The tunnel exit is marked with an asterisk. The polypeptide exit tunnel in mt-LSU is more proteinaceous than in bacteria as a result of two rRNA deletions. (**C**) Deletion of h7 in bacteria (gray) is compensated by changes to uL29 and an N-terminal extension of uL24. (**D**) Deletion of h24 (gray) results in the conserved β-hairpin of uL24 rotating closer to the tunnel exit and exposes uL22 to the nascent polypeptide.